Biosensors and Bioelectronics 117 (2018) 175–182

Contents lists available at ScienceDirect

Biosensors and Bioelectronics

journal homepage: www.elsevier.com/locate/bios

# Proton-ELISA: Electrochemical immunoassay on a dual-gated ISFET array

Duane S. Juang[a], Ching-Hui Lin[b], Yi-Ren Huo[a], Chia-Yu Tang[c], Chun-Ren Cheng[b], Hua-Shu Wu[b], Shih-Fen Huang[b], Alexander Kalnitsky[b], Chun-Cheng Lin[a,*]

[a] Department of Chemistry, National Tsing Hua University, 101, Section 2, Kuang-Fu Road, Hsinchu 30013, Taiwan
[b] Taiwan Semiconductor Manufacturing Company, 8, Li-Hsin Rd. 6, Hsinchu Science Park, Hsinchu 30077, Taiwan
[c] Institute of NanoEngineering and MicroSystems, National Tsing Hua University, 101, Section 2, Kuang-Fu Road, Hsinchu 30013, Taiwan

ARTICLE INFO

*Keywords:*
Biosensor
Immunoassay
ELISA
ISFET
Proton detection
Fenton's reaction

ABSTRACT

Here we report an electrochemical immunoassay platform called Proton-ELISA (H-ELISA) for the detection of bioanalytes. H-ELISA uniquely utilizes protons as an immunoassay detection medium, generated by the enzyme glucose oxidase (GOx) coupled with Fenton's reagent in a proton amplification reaction cascade that results in a highly amplified signal. A proton-sensitive dual-gated ion-sensitive field effect transistor (DG-ISFET) sensor was also developed for sensitive and accurate detection of the proton signal in H-ELISA. The DG-ISFET sensor comprises of a 128 × 128 array of 16,384 sensing transistors each with an individually addressable back gate to allow for a very high signal throughput and improved accuracy. We then demonstrated that the platform could detect C-reactive protein and immunoglobulin E down to concentrations of 12.5 and 125 pg/mL, respectively. We further showed that the platform is compatible with complex biological sample conditions such as human serum, suggesting that the platform is sufficiently robust for potential diagnostic applications.

## 1. Introduction

The enzyme-linked immunosorbent assay (ELISA) (Lequin, 2005) is the current gold standard for the detection of various biomarkers in scientific research and clinical diagnostics because of its high sensitivity, specificity and ability to directly assay complex biological samples such as blood serum without the need for analyte purification or enrichment. However, traditional ELISA relies on detection of optical absorbance or chemiluminescent signals, which may require large and costly optical machines for signal readout. This makes ELISA impractical for on-site rapid diagnostics in resource-limited settings. To realize the application of immunoassays in point-of-care diagnostics (Tarasov et al., 2016; Wan et al., 2013), there is a growing interest in developing non-optical based immunoassay platforms with a smaller footprint and lower cost. With the advantages of small component size, low cost, low power consumption, and rapid signal readout, electrical detection platforms (Ahmad et al., 2018; Grieshaber et al., 2008) have become popular approaches in the development of miniaturized immunoassays. Examples of electrical based biosensors include carbon nanotubes/graphene (Tiwari et al., 2016; Yang et al., 2010), silicon nanowires (Cui et al., 2001; Kim et al., 2016; Penner, 2012), zinc oxide (ZnO) nanowires (Vabbina et al., 2015), gold-based electrodes (Nidzworski et al., 2014), and a combination of the above (Paul et al., 2017). However, these electrical biosensor platforms still have to overcome challenges such as poorer sensitivity, accuracy, reproducibility, or fabrication costs, thus preventing their adoption in clinical diagnostics. Due to reliability concerns, there are currently very few electrical detection-based immunoassay platforms that have been approved by the U.S. Food and Drug Administration for clinical diagnostics.

One attractive platform for developing electrical biosensors is field effect transistors (FETs). FET-based platforms are widely explored for developing biosensors due to their fast response time, parallel sensing capability, sensitivity, and ease of integration with other semiconductor processes (Aliakbarinodehi et al., 2017; Kaisti, 2017; Sarangadharan et al., 2018). A particular type of FET sensor, the ion-sensitive field-effect transistor (ISFET) was first proposed by Bergveld in 1970 (Bergveld, 1970, 2003) and was originally intended as a pH/ion sensor (Hizawa et al., 2006). The platform is structurally similar to a conventional field effect transistor except that the physical dielectric gate is changed to a “floating gate” comprising of the liquid solution under interrogation, and can sensitively detect changes of charge in the liquid gate (Kaisti, 2017). ISFETs also share a lot of the similar architectures as CMOS (Complementary Metal–Oxide–Semiconductor) integrated circuits which are widely used in modern consumer electronics. Thus, they also share the same advantages of low production cost and high scalability. However, further attempts to develop an immunosensor platform based on ISFETs have not been very successful due to the Debye

* Corresponding author.
*E-mail address:* cclin66@mx.nthu.edu.tw (C.-C. Lin).

https://doi.org/10.1016/j.bios.2018.06.012
Received 26 March 2018; Received in revised form 22 May 2018; Accepted 5 June 2018
Available online 07 June 2018
0956-5663/ 

length ($\lambda_D$) limit (Lud et al., 2006; Stern et al., 2007) which predicts that the detectable electric potential at the ISFET surface decreases with a magnitude of 1/e for every increase by $\lambda_D$. As proteins and other biomolecules are generally large, with charge distributions outside or close to $\lambda_D$ limit, previous ISFET immunoassay platforms (Schoning and Poghossian, 2002; Zheng et al., 2005) have suffered from low sensitivities or require liquids of very low ionic strength for measurement. To extend the biosensing ability of ISFETs beyond $\lambda_D$ limit, we postulated that an indirect sensing method utilizing charged small ions as an intermediate sensing medium could enable the detection of biomolecules much larger than $\lambda_D$ on ISFET platforms.

In traditional ELISA, the final detection step employs an antibody tethered to an enzyme, most commonly horse radish peroxidase (HRP) or alkaline phosphatase (ALP), to catalyze the conversion of an optically inactive substrate into an optically active product for detection using a spectrophotometer. Previously, Jang et al. adopted an ALP tethered antibody to catalyze the reduction of silver ions ($Ag^+$) to Ag, which forms silver precipitates on the top of an ISFET biosensor surface to enhance immunoassay sensitivity (Jang et al., 2015). However, the silver precipitates render the device unrecyclable, thus one device can only be used for a single point measurement. Herein, we present an alternative electrochemical immunoassay platform termed Proton-ELISA (H-ELISA). Previously, the Ion Torrent semiconductor platform (Rothberg et al., 2011) was successfully used in DNA sequencing by directly sensing protons produced in enzymatic template-directed DNA synthesis. Inspired by this research, we designed H-ELISA by utilizing glucose as the substrate which is catalyzed by the enzyme glucose oxidase (GOx) to release protons ($H^+$) (Scheme 1) (Muller, 1928; Wong et al., 2008) that are detected by a proton-sensitive ISFET (Fig. 1). The use of protons as a detected medium provides advantages of rapid diffusion (even at low concentration) and easy removal from the biosensor surface without fouling the biosensor, thus permitting multiple measurements to be performed within a short time without the need for sensor regeneration. To further enhance the proton signal, the hydrogen peroxide ($H_2O_2$) byproduct released from the GOx catalyzed reaction was coupled with iron (II) sulfate ($FeSO_4$) to generate extra protons in the solution (data not shown). The mixture of $H_2O_2$ and $FeSO_4$ is commonly known as Fenton's reagent (Walling, 1975) and is used in industrial wastewater treatment (Kuo, 1992). The ferrous ion ($Fe^{2+}$) in Fenton's reagent reacts with $H_2O_2$ via a hydroxyl radical transfer mechanism, which consumes the $H_2O_2$ byproduct generated by the GOx catalyzed reaction, thus further pushing the reaction toward the product side. Although the net reaction is not clear, the addition of $FeSO_4$ results in an increase of $H^+$ concentration. It is also worth noting that the reagents (glucose and $FeSO_4$) used in the H-ELISA system are of very low cost, readily available, and highly stable at room temperature, which is highly advantageous in assay implementation.

Our ISFET transistor employs a dual-gated design that allows the highly sensitive detection of pH changes near the Nernstian maximum limit of 59 mV/pH at 25 °C, as predicted by the Nernst equation (Knopfmacher et al., 2010). Unlike early ISFET designs that only contain a single floating gate architecture, the dual-gated ISFET (DG-ISFET) (Duarte-Guevara et al., 2014; Huang et al., 2015; Khamaisi et al., 2010; Knopfmacher et al., 2010) design comprises two gates: a dielectric top gate biased with a reference electrode and a bottom gate composed of a buried oxide layer. The two coupled gates in our device enable higher signal stability as the bottom gate can be used for fixing the surface voltage of the transistors during measurement. This feature is important in biosensing applications because the detectable changes in surface charge are usually very small. Moreover, accuracy is a critical concern for performing sensitive electrical measurements because the signal is often weak and close to the background noise, a common issue that often affects electrical biosensor platforms. We employed two strategies in designing the DG-ISFET to improve detection accuracy. First, simply increasing the sampling number (n) can increase statistical significance to obtain a higher signal-to-noise ratio for weak signals. Thus, our device was designed with an array of 128 × 128 = 16,384 sensing transistors to allow for a very high signal throughput. This essentially averages out variations between different transistors and enables better signal accuracy. This feature of our device significantly improves on the poor accuracy encountered in previous ISFET detection platforms, which commonly contain only one sensing transistor. Second, in contrast to previous DG-ISFET designs in which all transistors on the same chip share a single common back gate, our device was designed to have each sensing transistor paired with a corresponding individually addressable back gate. This enables the tailored biasing of each transistor to normalize errors which arise from fabrication inconsistencies across the wafer surface and to ensure that all transistors operate across a uniform playing field. In summary, by combining a proton-based sensing method and the DG-ISFET array allowed us to achieve higher sensitivity than that of traditional optical ELISA and simultaneously afforded the advantages of a small detection platform footprint and cost efficacy.

## 2. Materials and methods

### 2.1. DG-ISFET device fabrication

Fabrication of the DG-ISFET devices was carried out by Taiwan Semiconductor Manufacturing Company (TSMC, Taiwan) using a 0.18 μm system on chip (SOI) technology with a novel two-substrate approach. In brief, a conventional CMOS transistor was fabricated on a SOI substrate comprising of a polysilicon (back) gate, a $SiO_2$ gate dielectric, and oppositely doped source and drain areas. Electrical connections to the source, drain and gates were established via patterning of aluminum and copper conducting wires to form multilayer interconnects, then insulated using $SiO_2$ interposing dielectric layers. This SOI wafer was then flipped over and bonded via the front side (containing the connecting wires and dielectric layer) to another wafer substrate (carrier wafer). In this way, the CMOS transistor with the back gate was buried between two wafer substrates: the original SOI wafer and a carrier wafer. The bulk silicon on the back of the original SOI wafer was then removed via a chemical mechanical polish process to expose the buried silicon oxide layer on the SOI wafer. The active sensing regions buried underneath the oxide layer were then exposed via lithography and wet etching to form a sensing window, whereas the source and drain regions remained protected by the oxide layer. A high-k film of hafnium oxide was then deposited on the wafer surface to serve as the top fluid-gate dielectric and the sensing interface between the fluid and the transistor. Hafnium oxide was chosen for its near-Nernstian ideal electrical response characteristics (Lee et al., 2000). Lastly, the device was packaged to allow for easy portable

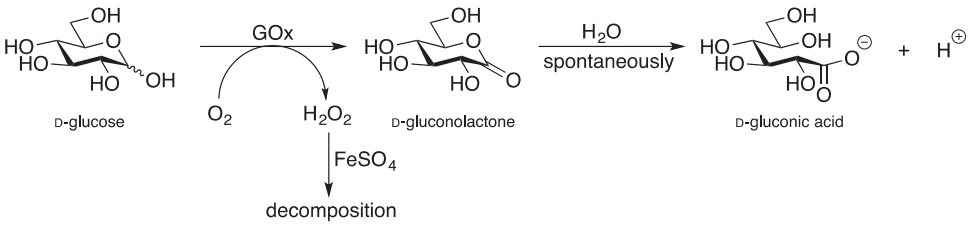


**Scheme 1.** GOx catalyzed generation of protons. GOx catalyzes the oxidation of D-glucose to D-gluconolactone, which is further hydrolyzed in the presence of water to D-gluconic acid, releasing one proton and one molecule of $H_2O_2$ per molecule of D-glucose oxidized. The presence of $FeSO_4$ consumes the $H_2O_2$, thus further pushing the reaction toward the product side.

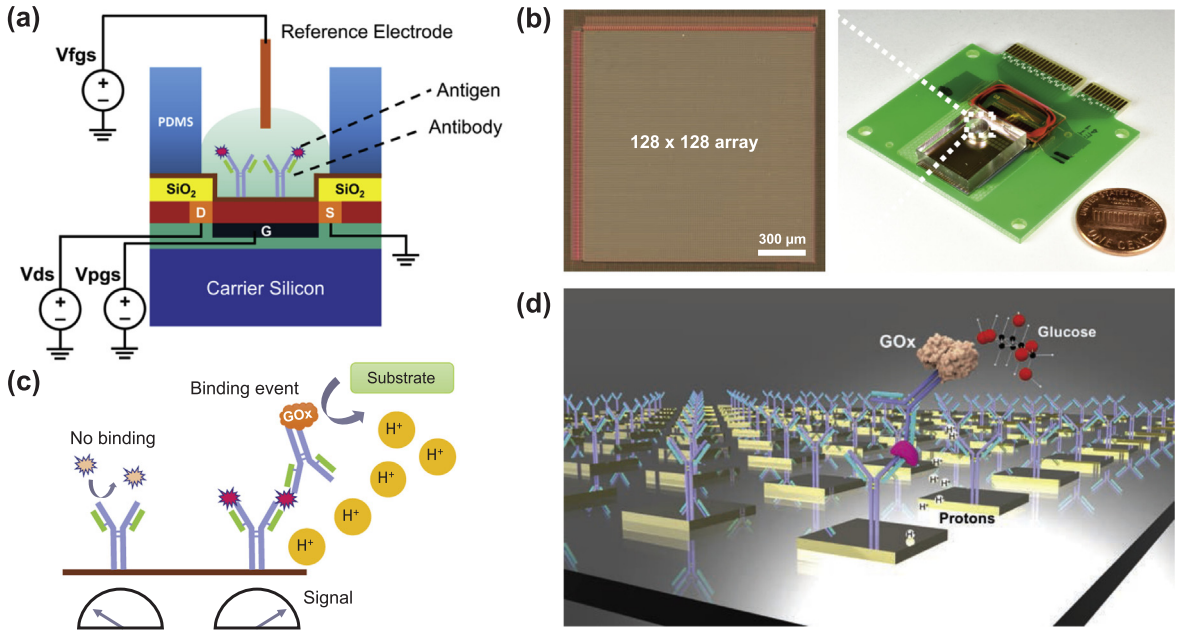


**Fig. 1.** Setup of the H-ELISA platform. (a) Schematic of the DG-ISFET biosensor. The dielectric layer comprises a high-K hafnium oxide material and is covalently functionalized with capture antibodies specific for target antigens. (b) Whole-device and close-up images of the DG-ISFET chip. (c) Schematic of the sensing principle of the H-ELISA platform. Upon binding of the antigen of interest to the capture antibody, a detection antibody coupled with GOx is added to form a sandwich complex on the sensing surface. The enzyme substrate (glucose with $FeSO_4$) is added and subsequently forms gluconic acid and protons ($H^+$), which can be detected by the DG-ISFET device. (d) Rendered image summarizing the principle of the H-ELISA platform.

measurements using a plug-and-play acquisition platform (Fig. S1 in the supporting information).

### 2.2. DG-ISFET measurement setup

Electrical measurements of the DG-ISFET devices was performed using a custom-built acquisition platform (Fig. S1) connected to a computer running an in-house developed program written with LabVIEW (National instruments, USA). Connecting the DG-ISFET device to the acquisition platform was done by simply plugging the connector pins on the packaged DG-ISFET device into the socket of the acquisition platform. To allow liquid to be held on top of the sensing surface, a 4 mm thick polydimethylsiloxane (PDMS) slab with a 6 mm diameter circular reservoir was mounted on the chip surface via physical adhesion, which could accommodate a volume of approx. 100 µL of liquid without spilling over. A leak-free Ag/AgCl reference electrode (Warner Instruments, Hamden, CT) was inserted into the reservoir but without touching the sensor surface to provide a voltage bias for fixing the fluid potential during measurements. The fluid top gate was given a 2.0 V bias via the reference electrode for performing all fixed bias measurements, whereas the back gate was given a voltage of 0 V to fix the electric potential. Prior to electrical measurements, a 120 s delay was implemented to allow the current to stabilize and to minimize effects of drift after applying the gate voltage from the reference electrode. To calculate the noise and standard deviation of measurements in each experiment, 16 loops of measurements were performed, with each loop lasting approx. 2 s.

### 2.3. Functionalization of ISFET chip with antibodies

For immobilization of antibodies onto the DG-ISFET sensor, the sensing surface was hydroxylated with 10% $H_2O_2$ at room temperature (RT) overnight, followed by washing and incubation with 2.5% 3-aminopropyltriethoxysilane (APTES) in 99% ethanol at RT for 1 h to functionalize the surface with amine. The chip was subsequently washed with ethanol, blown dry with nitrogen, and incubated with 2.5% glutaraldehyde in PBS (phosphate-buffered saline) at RT for 1 h to change the surface functionality to aldehyde via imine formation. After being washed with $ddH_2O$, the chip was incubated with capture antibody (anti-CRP antibody at 2 µg/mL) in PBS at RT for 1 h.

### 2.4. Real-time H-ELISA

The antibody functionalized chips were blocked with 1% BSA (bovine serum albumin) for 1 h, washed with PBST (phosphate buffered saline with 0.05% Tween-20), and then incubated with samples (diluted antigen standards or serum samples) at RT for 2 h. After washing with PBST for 3 times, detection antibodies (anti-CRP antibody at 90 ng/mL) in 1% BSA were added and incubated at RT for 1 h. The chips were washed again with PBST and then incubated with 10 µg/mL of avidin conjugated GOx for 30 min. The chips were then washed with PBST and then with 50 mM potassium chloride (KCl) solution for 3 times each to remove any potential residual PBS buffer which might interfere with pH detection. An electrical measurement was performed at this step using 25 mM KCl and 250 µg/mL $FeSO_4$ to serve as a background blanking signal with the reference electrode providing a voltage bias of 2.0 V. It's worth to note that $FeSO_4$ is slightly acidic. Thus, the blank measurements were taken in the presence of $FeSO_4$. The enzyme substrate (3 mg/mL glucose in 25 mM KCl solution and 250 µg/mL $FeSO_4$) was added, followed by electrical measurement to detect the generation of protons as a function of antigen concentration.

## 3. Results and discussions

### 3.1. Chip design and fabrication

The DG-ISFET array was designed with an array of 128 × 128 = 16,384 sensing transistors (Fig. S1 and S2). In order to normalize any potential background interference, 128 dummy pixels were incorporated across the diagonal of the DG-ISFET sensing array to serve as a negative background control (Fig. S2). Data from these pixels were excluded from the calculation of the mean chip output current. Electrical signals of the DG-ISFET were measured using a custom-built acquisition platform (Fig. S1) connected to a computer running an in-

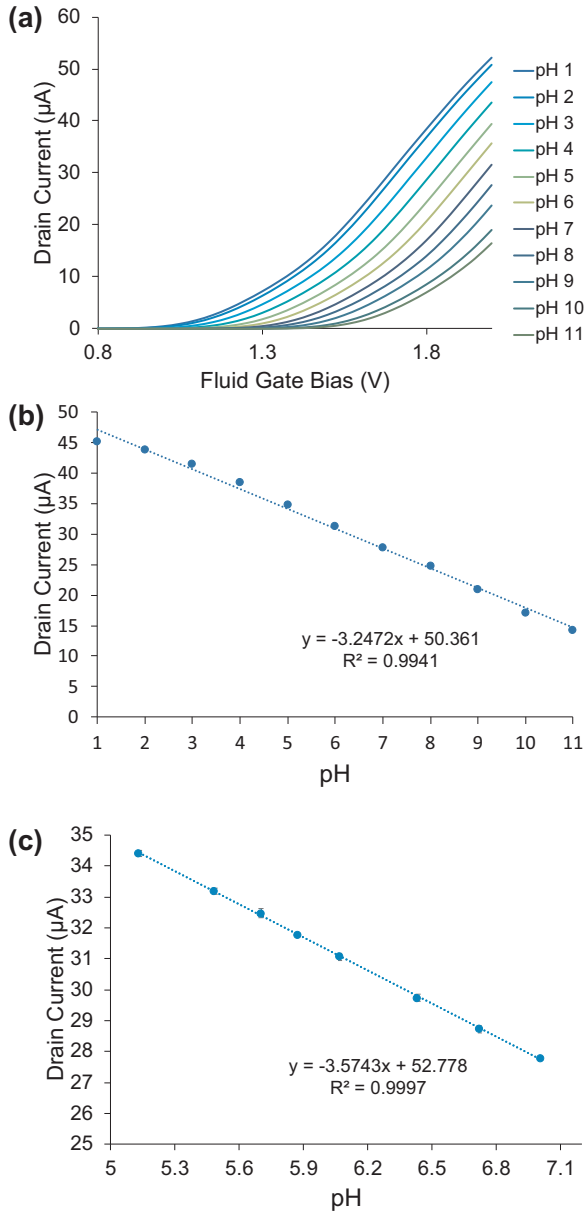


**Fig. 2.** pH sensitivity response of the DG-ISFET device. (a) Voltage/current response of the DG-ISFET device swept with a top gate bias from 0 V to 2.0 V for pH standard buffers ranging from pH 1 to pH 11. The back gate was held constant at 0 V. (b) Current response for pH buffer standards ranging from pH 1–11 with a linear regression curve. Fluid top gate bias: 2.0 V, back gate: 0 V. (c) Current response for a pH titration of pH 7.00 standard buffer with HCl ranging from pH 7.00 to pH 5.13. Fluid top gate bias: 2.0 V, back gate: 0 V.

house developed program, which allows users to control measurement parameters such as the top (fluid) gate voltage (Vfgs), back (poly) gate voltage (Vpgs), wait time, and acquisition time. The acquisition platform sequentially scanned through each transistor on the DG-ISFET row by row at a very fast rate, enabling the measurement of all 16,384 transistors within 2–3 s. This speed was especially valuable since it enabled using the platform as a real-time biosensing device for performing time-dependent studies. To calculate the standard deviation of measurement in each experiment, 16 loops of measurement were performed, with each loop lasting approx. 2 s. A 120 s delay prior to measurement was implemented to allow the current to stabilize and to minimize effects of drift after applying the gate voltage from the reference electrode.

### 3.2. Characterization and pH response of the DG-ISFET sensor

To characterize the linearity of the current response to pH change, the device was screened with pH standard calibration buffers (CertiPUR buffer solution, Millipore, Germany) ranging from pH 1–11 (Fig. 2a), with the drain current plotted against pH in a scatter plot with a linear regression line. The voltage/current response to pH exhibited a highly linear relationship, with a linear fit $R^2$ value of 0.9941 (Fig. 2b). To further confirm the accuracy of the device in measuring the pH change over a narrow range, seven HCl titrations of a pH 7.00 standard buffer (BDH pH reference standard buffer, VWR International, USA) were performed to obtain 8 solutions of known pH ranging from pH 7.00 to pH 5.13. After measuring the pH solutions with DG-ISFET device, the output current was plotted against pH, which was calibrated using a benchtop pH meter equipped with a double-junction pH electrode (InLab Ultra-Micro-ISM, Mettler-Toledo, Switzerland). The results showed that the current response of the DG-ISFET chip to pH was indeed highly linear, with a linear fit $R^2$ value of 0.9997 (Fig. 2c).

To evaluate the accuracy and repeatability of the device, standard buffers at pH 7 and pH 8 were measured 20 times. The current response varied only slightly between measurements, with a coefficient of variance (CV) of 0.43% and 0.23% for pH 7 and pH 8, respectively (Fig. 3a). Moreover, intra-chip variation between pixels was also low, albeit slightly higher than the variation between individual measurements, with a CV of 1.78% for pH 7% and 1.82% for pH 8 (Fig. 3b). Three different pixels distributed across the sensing chip at the bottom left (pixel 0,0), center (pixel 64,64) and upper right (pixel 128,128) corners were selected to evaluate the consistency of the voltage/current response of the chip. The results showed nearly identical voltage/current response for these three pixels (Fig. 3c). In addition, the voltage/current response was also highly consistent regardless of the direction of the applied voltage (i.e., forward: 0–2.0 V or reverse: 2.0–0 V), showing very little hysteresis (Fig. 3d). Thus, the developed DG-ISFET device can offer highly accurate pH measurements, both in repeatability and intra-chip consistency. It's worth to note that the pH sensitivity and resolution of different fabricated devices are also highly consistent (Fig. S3), although we did observe minor device to device variations in drain current values when measuring the same pH solution, which can be normalized through pH calibration.

### 3.3. GOx coupled with Fenton's reaction for enhanced proton generation

As shown above, the developed DG-ISFET device is highly sensitive for detecting different proton concentrations (pH). However, protons are rapidly quenched in buffered solutions such as PBS. Thus, a GOx-catalyzed reaction (Scheme 1) was adopted for generating a proton signal in an unbuffered deionized water solution. Although the GOx showed good activity in pure water, the conductivity of the deionized water was too low to accurately measure protons with the DG-ISFET chip. To enhance the conductivity of the solution, various concentrations of KCl were evaluated as a supporting electrolyte in the GOx catalyzed reaction solution. Results showed that the proton-generating activity of GOx slightly decreased in response to increasing KCl concentration (Fig. S4). However, at 25 mM KCl solution, GOx activity was only very slightly decreased, but allowed for a stable measurement of proton signal. Thus, this KCl concentration was used in all subsequent measurements.

To enhance the sensitivity of the H-ELISA detection method, various strategies coupled with the GOx were attempted to efficiently generate protons, since the limiting factor in the final detection step is the number of protons that can be generated by the very few enzymes bound to the surface. The activities of enzymes are known to diminish in response to product accumulation as a natural feedback-inhibition mechanism (Bao et al., 2003; Kleppe, 1966). Thus, an effective way to enhance enzymatic activity is to remove the product from the reaction. $FeSO_4$ was previously reported to react with $H_2O_2$, a byproduct of the

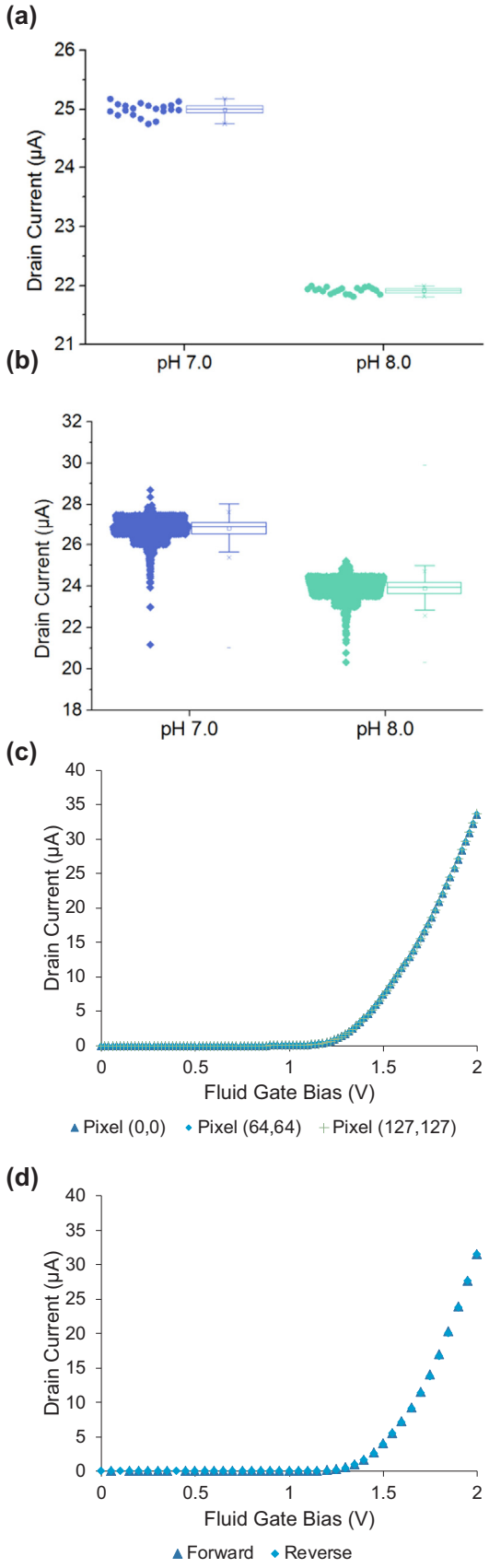


**Fig. 3.** Accuracy and repeatability of DG-ISFET chip. (a) Current responses of 20 repeated measurements of pH 7 and pH 8 standard buffers using the DG-ISFET chip. Fluid top gate bias: 2.0 V, back gate: 0 V. (b) Current response of each individual sensing pixel within one chip for pH 7 and pH 8 standard buffers. Fluid top gate bias: 2.0 V, back gate: 0 V. (c) Voltage/current response of three different pixels distributed across the sensing chip at the bottom left (pixel 0,0), center (pixel 64,64), and upper right (pixel 128,128) corners when the fluid top gate bias was swept from 0 V to 2.0 V, with the back gate held constant at 0 V. (d) Measurement of the voltage/current response of the chip when the fluid top gate bias was swept in the forward (0–2.0 V) or reverse (2.0–0 V) direction, with the back gate held constant at 0 V.

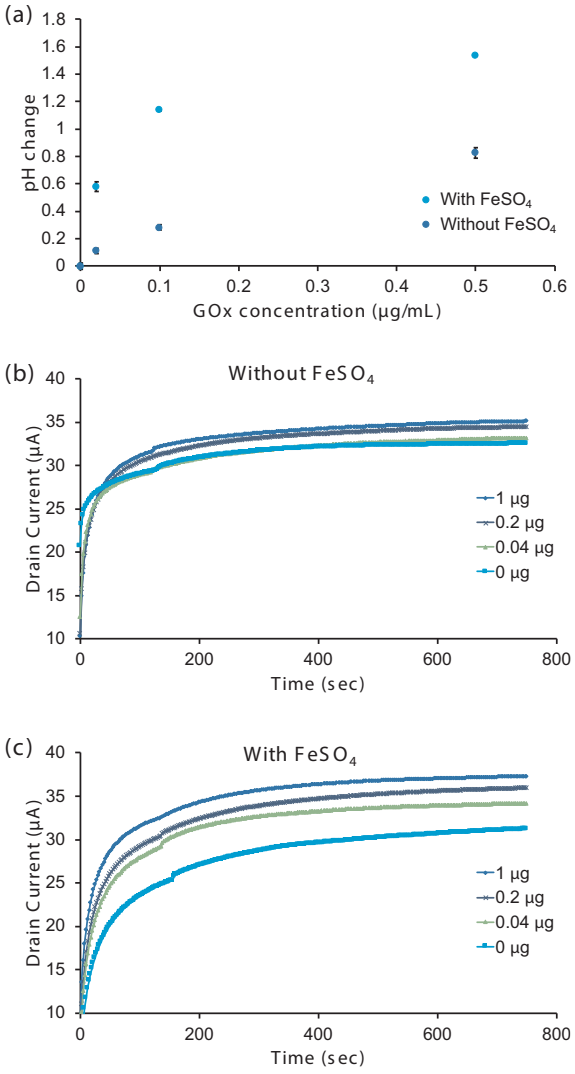


**Fig. 4.** Enhancement in proton generation by $FeSO_4$. (a) Adding $FeSO_4$ can increase proton generation with the same concentration of GOx. (b) Real-time measurement of proton generation with various GOx concentrations over 750 s (b) without and (c) with $FeSO_4$ in the reaction solution over a 750 s period.

oxidation of glucose by GOx, to form $H_2O$ and $O_2$ in a process known as Fenton's reaction (Walling, 1975). During Fenton's reaction, the ferrous ion ($Fe^{2+}$) in $FeSO_4$ reacts with $H_2O_2$ via a hydroxyl radical transfer mechanism. This process consumes $H_2O_2$ and moves the reaction toward the product side (Le Chatelier's principle). The efficiency of proton generation by GOx with or without the addition of $FeSO_4$ was evaluated by a five-fold serial dilution of GOx, followed by addition of the glucose substrate. Impressively, including 250 μg/mL (1.65 mM) of $FeSO_4$ in the reaction mixture resulted in a 515% enhancement in the proton generation efficiency, as revealed by the change in pH (Fig. 4a), suggesting

that this strategy is highly effective. In addition, no side reactions occurred between $FeSO_4$ and glucose, as no change in pH was observed without the addition of GOx (Fig. S5). We also used various glucose concentrations to evaluate its effect in the reaction and found that a 3 mg/mL concentration of glucose provides sufficient substrate for a large pH change in the GOx catalyzed reaction without significantly increasing liquid viscosity (Fig. S6). It should be noted that even though hydroxyl radicals ($^{\bullet}OH$) are generated in Fenton's reaction, the active $^{\bullet}OH$ species do not appear to affect the overall efficiency of proton production. Notably, $FeSO_4$ showed better enhancement of proton production in the GOx-catalyzed reaction than that of potassium ferricyanide, $K_3[Fe(CN)_6]$, which is a commonly used additive in conventional glucose meters to replace oxygen as the electron donor (Shulga et al., 1994) (Data not shown).

### 3.4. Detection of GOx-catalyzed proton generation using the DG-ISFET sensor

A powerful feature of the DG-ISFET chip is the ability to measure a pH change in real time, which is highly useful for quantifying enzyme kinetics and real-time monitoring of the reaction process. GOx proton generation was detected in real time using the DG-ISFET detector in continuous measurement mode, wherein the detector sequentially scanned through all the pixels on the chip, with each scan lasting approx. 2 s. To measure the GOx enzyme activity, a GOx enzyme solution was added to the reservoir above the DG-ISFET sensor, followed by the addition of glucose substrate solution (3 mg/mL) with or without $FeSO_4$ at 250 μg/mL. The drain current was immediately measured for 600 s. The results showed that the addition of $FeSO_4$ in the substrate solution dramatically increased the change in the drain current with the increasing enzyme concentration in the reaction solution (Fig. 4b and c), which is consistent with the trend of the change in pH (Fig. 4a).

### 3.5. Real-time H-ELISA

To demonstrate the applicability of the H-ELISA platform, we chose C-reactive protein (CRP), a clinically accepted biomarker for detecting possible acute infections or inflammatory responses as a model analyte (Bryan et al., 2013; Delfino et al., 2008; Kim et al., 2013). To fabricate the desired device, capture antibodies were immobilized onto the sensing surface as described in the experimental section using a modified protocol from a previously reported method (Juang and Hsu, 2016). To perform the immunoassays, the antibody-functionalized chips were sequentially incubated with serially diluted CRP standard samples (50–0 pg/mL), biotinylated anti-CRP antibody, and avidin-conjugated GOx. Prior to measurement, the chip was washed with PBST and 25 mM KCl solution for 3 times to remove any residual PBS buffer that might interfere with pH detection. An electrical measurement was then performed using a solution of 25 mM KCl and 250 μg/mL $FeSO_4$ to serve as a background blanking step. The enzyme substrate (100 μL of 3 mg/mL glucose in 25 mM KCl solution and 250 μg/mL $FeSO_4$) was added, and measurements were started immediately using the real-time acquisition mode of the software to detect the generated protons as a function of the antigen concentration. We easily obtained a detectable signal down to 25 pg/mL of CRP analyte (Fig. 5a). However, we noticed that the signal was prone to drift and lacked stability during the continuous acquisition period of H-ELISA (Fig. 5a), a phenomenon that we did not observe with the bare chip (i.e., without antibody modification) in continuous measurements, such as those in Fig. 4b and c. We postulated that this likely resulted from the fouling of the sensor surface due to the immobilization and adsorption of proteins such as the antibody and BSA, which have been reported to cause fouling and inefficient charge transfer in electrochemical devices (Glavan et al., 2014). Additionally, the multiple rigorous washing and incubation steps of the immunoassay might also contribute to variations in the sensing surface and the reduced signal stability. Moreover, as the antibodies are covalently attached to the sensor surface, regenerating the sensor would be difficult in this approach as it would require very harsh chemical conditions to fully remove the attached antibodies which could also damage the sensor.

### 3.6. Endpoint H-ELISA

Due to the above described complications, we reasoned that decoupling the binding and reaction steps from the final detection step to be performed on the DG-ISFET could circumvent issues associated with biosensor surface fouling. We therefore performed all the steps of the H-ELISA experiment as described above off-chip in a conventional 96-well ELISA microtiter plate, except the final detection step which was performed on chip. After adding the glucose substrate solution to the plate and incubating for 15 min at 37 °C, the reaction solution was transferred from the plate onto the DG-ISFET chip for proton detection. In this setup, the DG-ISFET chip did not require chemical modification and conjugation with antibodies; instead, it was only used to detect the protons generated during the H-ELISA assay. In addition to offering reduced detection complications from fouling of the sensing surface, this method also affords a lower cost per assay due to the reduced consumption of DG-ISFET sensors. Because we were able to reuse the same chip for detecting multiple samples, this approach provides higher accuracy and better precision as there was no chip-to-chip variation. This new protocol was applied on the detection of two biomarkers, C-reactive protein (CRP) and immunoglobulin E (IgE), biomarkers for inflammation (Bryan et al., 2013; Delfino et al., 2008; Kim et al., 2013) and allergic responses (Matsui et al., 2010), respectively. Although the antibody-antigen complex was decoupled from the DG-ISFET surface, the results showed that the binding and reaction steps of H-ELISA could indeed be operated off-chip while retaining the detection sensitivity of the chip (Fig. 5b). Using this method, we were able to detect CRP and IgE down to a concentration of 12.5 pg/mL and 125 pg/mL, respectively (Fig. 5b), which are more sensitive than those observed in traditional optical ELISA using the same antibody-antigen pairs (Fig. S7). Although the current setup still requires manual liquid handling of samples and reagents, future studies may focus on integrating microfluidic channels and microwell structures with the DG-ISFET sensor to enable automated and high-throughput liquid handling for the analysis of multiple samples in the same device and to reduce sample consumption.

To demonstrate the detection of biomarkers in serum samples with the current platform, we assayed the concentration of CRP from three healthy donors using our H-ELISA platform and conventional ELISA as a comparison. The results showed that both methods yielded similar protein concentrations, with H-ELISA showing a slightly lower concentration, possibly due to differences in the signal amplification and detection of these two methods. It should be noted that the sensitivity of our platform allows the detection of CRP in serum using a very small sample volume (1 μL of serum diluted 10,000 times, although theoretically only 10 nL of serum is needed), suggesting that blood samples collected from a finger prick would be more than sufficient for CRP detection using our platform. Overall, the results suggest that the H-ELISA platform is a potential diagnostic method for detecting disease markers in human serum.

## 4. Conclusion

In summary, we demonstrated a non-optical electrochemical immunoassay system using protons as a detection medium coupled with a high-throughput DG-ISFET sensor. In this work, we pioneered the coupling of Fenton's reagent with GOx to enhance production of proton ions. The conjunction of the proton amplification system with a high-density DG-ISFET sensor array provides sensitive and reliable signal acquisition. Although the current device uses only one sensing chamber to cover the whole area of the sensing array, it can be easily scaled up to

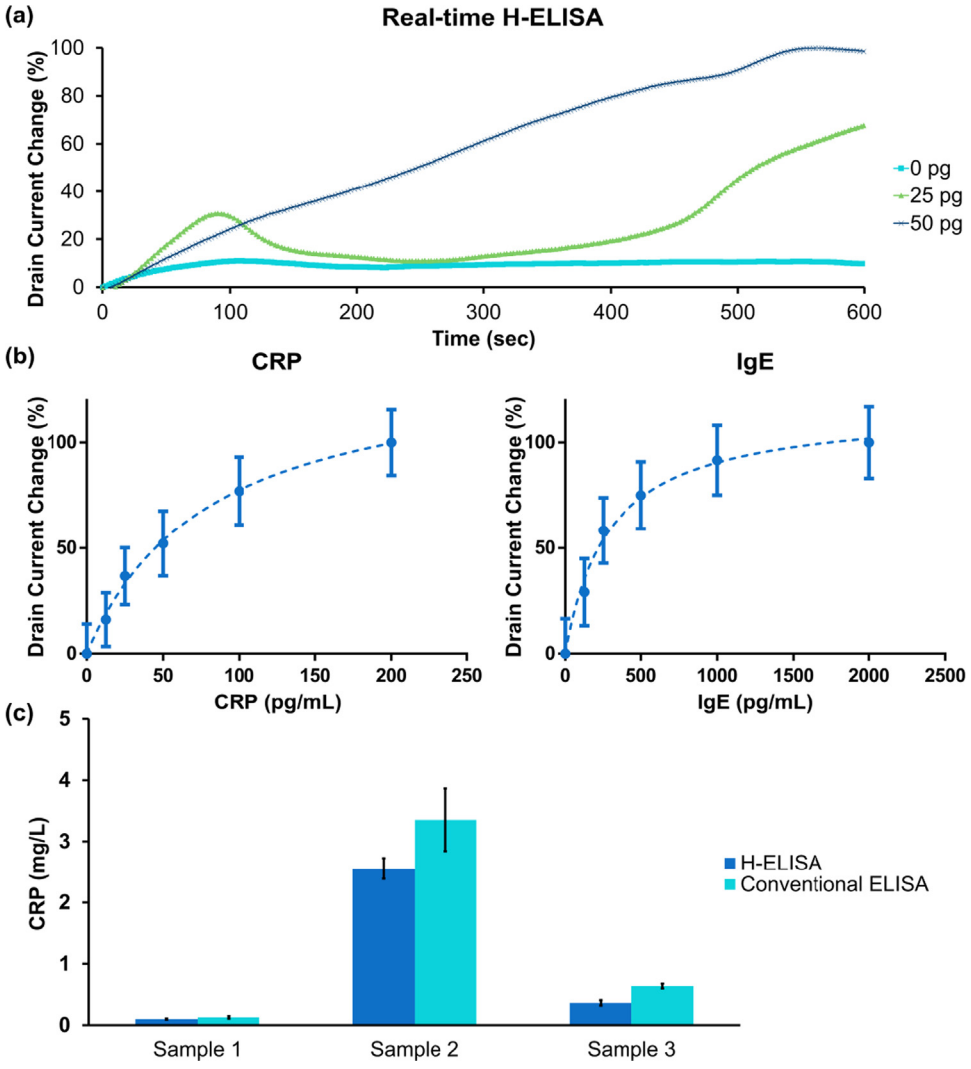


**Fig. 5.** Real-time and end-point H-ELISA. (a) Real-time H-ELISA. Capture antibodies were directly immobilized onto the DG-ISFET chip surface, followed by antigen capture and labeling. After adding the glucose substrate, proton detection was performed for 600 s (b) End-point H-ELISA on 96-well plates. CRP, IgE and CRP antigens were serially diluted 5 times ranging from 200 to 0 pg/mL and 2000–0 pg/mL, respectively. Error bars represent the intra-chip standard deviation of the sensing pixels within each measurement. (c) Quantification of CRP concentration in serum samples from three healthy donors using H-ELISA and conventional ELISA. These two methods gave similar results, with H-ELISA showing a slightly lower concentration. Error bars denote the standard deviation of 2 technical replicates.

a multiplex well format for high-throughput screening (Chen et al., 2008; Juang and Hsu, 2016; Phizicky et al., 2003) by taking advantage of the simplicity and cost-effectiveness of scaling up semiconductor manufacturing technologies. Furthermore, although the size of the current sensing platform is already portable (Fig. S1), we envision that it could be easily further scaled down to the size and weight of a handheld device, enabling its application as a point-of-care testing tool. The high sensitivity and real-time high signal throughput of the ISFET also suggest that the developed device is potential to be applied in other biosensing assays such as nucleic acid detection, metabolite analysis, and even binding/kinetic assays.

ISFET platforms have also shown potential for the label-free multiplex detection of biomolecules if the capture antibody is immobilized on the surface. However, such direct sensing platforms are usually lower sensitivity, more prone to false positives, and high background noise. By contrast, H-ELISA affords lower incidence of false positives due to the use of a sandwich ELISA format, in which a single antigen requires the binding of two different antibodies in order to have a positive signal, thus conferring much higher fidelity and specificity. In addition, the GOx-$FeSO_4$ signal amplification system in H-ELISA enables much greater enhancement of detection sensitivity compared to direct sensing methods. Thus, developing methods that can combine the advantages of multiplex and high-throughput screening with the sensitivity and specificity of our H-ELISA platform will be of considerable interest in the future.

## Acknowledgement

We would like to acknowledge Dr. Chia-Hsien Hsu and Mr. Hui-Ying Lin at National Health Research Institute in Zhunan, Taiwan, as well as Mrs. Jui-Cheng Huang and Ching-Hua Wen at TSMC for providing valuable insights and technical support. This work was supported by the Ministry of Science and Technology of Taiwan (104-2113-M-007-006-MY3) and in part by a Joint Development Project grant provided by TSMC (106A0167EW).

## Competing financial interests

The authors declare no competing financial interest.

## Appendix A. Supporting information

Supplementary data associated with this article can be found in the online version at http://dx.doi.org/10.1016/j.bios.2018.06.012.

## References

Ahmad, R., Mahmoudi, T., Ahn, M.S., Hahn, Y.B., 2018. Biosens. Bioelectron. 100, 312–325.
Aliakbarinodehi, N., Jolly, P., Bhalla, N., Miodek, A., De Micheli, G., Estrela, P., Carrara, S., 2017. Sci. Rep. 7.
Bao, J., Furumoto, K., Yoshimoto, M., Fukunaga, K., Nakao, K., 2003. Biochem. Eng. J. 13, 69–72.

Bergveld, P., 1970. IEEE Trans. Biomed. Eng. BME 17, 70–71.
Bergveld, P., 2003. Sens Actuators B: Chem. 88, 1–20.
Bryan, T., Luo, X., Bueno, P.R., Davis, J.J., 2013. Biosens. Bioelectron. 39, 94–98.
Chen, M.L., Adak, A.K., Yeh, N.C., Yang, W.B., Chuang, Y.J., Wong, C.H., Hwang, K.C., Hwu, J.R.R., Hsieh, S.L., Lin, C.C., 2008. Angew. Chem. Int. Ed. 47, 8627–8630.
Cui, Y., Wei, Q., Park, H., Lieber, C.M., 2001. Science 293, 1289–1292.
Delfino, R.J., Staimer, N., Tjoa, T., Polidori, A., Arhami, M., Gillen, D.L., Kleinman, M.T., Vaziri, N.D., Longhurst, J., Zaldivar, F., Sioutas, C., 2008. Environ. Health Perspect. 116, 898–906.
Duarte-Guevara, C., Lai, F.L., Cheng, C.W., Reddy Jr., B., Salm, E., Swaminathan, V., Tsui, Y.K., Tuan, H.C., Kalnitsky, A., Liu, Y.S., Bashir, R., 2014. Anal. Chem. 86, 8359–8367.
Glavan, A.C., Christodouleas, D.C., Mosadegh, B., Yu, H.D., Smith, B.S., Lessing, J., Fernandez-Abedul, M.T., Whitesides, G.M., 2014. Anal. Chem. 86, 11999–12007.
Grieshaber, D., MacKenzie, R., Voros, J., Reimhult, E., 2008. Sensors 8, 1400–1458.
Hizawa, T., Sawada, K., Takao, H., Ishida, M., 2006. Sens Actuators B: Chem. 117, 509–515.
Huang, Y.J., Lin, C.C., Huang, J.C., Hsieh, C.H., Wen, C.H., Chen, T.T., Jeng, L.S., Yang, C. K., Yang, J.H., Tsui, F., Liu, Y.S., Liu, S., Chen, M., 2015. 2015 IEEE International Electron Devices Meeting (IEDM), 29.2.1-29.2.4.
Jang, H.J., Ahn, J., Kim, M.G., Shin, Y.B., Jeun, M., Cho, W.J., Lee, K.H., 2015. Biosens. Bioelectron. 64, 318–323.
Juang, D.S., Hsu, C.H., 2016. Lab Chip 16, 459–464.
Kaisti, M., 2017. Biosens. Bioelectron. 98, 437–448.
Khamaisi, B., Vaknin, O., Shaya, O., Ashkenasy, N., 2010. Acs Nano 4, 4601–4608.
Kim, C.H., Ahn, J.H., Kim, J.Y., Choi, J.M., Lim, K.C., Park, T.J., Heo, N.S., Lee, H.G., Kim, J.W., Choi, Y.K., 2013. Biosens. Bioelectron. 41, 322–327.
Kim, K., Park, C., Kwon, D., Kim, D., Meyyappan, M., Jeon, S., Lee, J.S., 2016. Biosens. Bioelectron. 77, 695–701.
Kleppe, K., 1966. Biochemistry 5, 139–143.
Knopfmacher, O., Tarasov, A., Fu, W.Y., Wipf, M., Niesen, B., Calame, M., Schonenberger, C., 2010. Nano Lett. 10, 2268–2274.
Kuo, W.G., 1992. Water Res. 26, 881–886.
Lee, B.H., Kang, L.G., Nieh, R., Qi, W.J., Lee, J.C., 2000. Appl. Phys. Lett. 76, 1926–1928.
Lequin, R.M., 2005. Clin. Chem. 51, 2415–2418.
Lud, S.Q., Nikolaides, M.G., Haase, I., Fischer, M., Bausch, A.R., 2006. Chemphyschem 7, 379–384.
Matsui, E.C., Sampson, H.A., Bahnson, H.T., Gruchalla, R.S., Pongracic, J.A., Teach, S.J., Gergen, P.J., Bloomberg, G.R., Chmiel, J.F., Liu, A.H., Kattan, M., Sorkness, C.A., Steinbach, S.F., Story, R.E., Visness, C.M., Consortium, I.-C.A., 2010. Allergy 65, 1414–1422.
Muller, D., 1928. Biochem. Z. 199, 136–170.
Nidzworski, D., Pranszke, P., Grudniewska, M., Krol, E., Gromadzka, B., 2014. Biosens. Bioelectron. 59, 239–242.
Paul, K.B., Singh, V., Vanjari, S.R., Singh, S.G., 2017. Biosens. Bioelectron. 88, 144–152.
Penner, R.M., 2012. Annu Rev. Anal. Chem. 5, 461–485.
Phizicky, E., Bastiaens, P.I.H., Zhu, H., Snyder, M., Fields, S., 2003. Nature 422, 208–215.
Rothberg, J.M., Hinz, W., Rearick, T.M., Schultz, J., Mileski, W., Davey, M., Leamon, J.H., Johnson, K., Milgrew, M.J., Edwards, M., Hoon, J., Simons, J.F., Marran, D., Myers, J.W., Davidson, J.F., Branting, A., Nobile, J.R., Puc, B.P., Light, D., Clark, T.A., Huber, M., Branciforte, J.T., Stoner, I.B., Cawley, S.E., Lyons, M., Fu, Y., Homer, N., Sedova, M., Miao, X., Reed, B., Sabina, J., Feierstein, E., Schorn, M., Alanjary, M., Dimalanta, E., Dressman, D., Kasinskas, R., Sokolsky, T., Fidanza, J.A., Namsaraev, E., McKernan, K.J., Williams, A., Roth, G.T., Bustillo, J., 2011. Nature 475, 348–352.
Sarangadharan, I., Regmi, A., Chen, Y.W., Hsu, C.P., Chen, P.C., Chang, W.H., Lee, G.Y., Chyi, J.I., Shiesh, S.C., Lee, G.B., Wang, Y.L., 2018. Biosens. Bioelectron. 100, 282–289.
Schoning, M.J., Poghossian, A., 2002. Analyst 127, 1137–1151.
Shulga, A.A., Koudelkahep, M., Derooij, N.F., Netchiporouk, L.I., 1994. Anal. Chem. 66, 205–210.
Stern, E., Wagner, R., Sigworth, F.J., Breaker, R., Fahmy, T.M., Reed, M.A., 2007. Nano Lett. 7, 3405–3409.
Tarasov, A., Gray, D.W., Tsai, M.Y., Shields, N., Montrose, A., Creedon, N., Lovera, P., O'Riordan, A., Mooney, M.H., Vogel, E.M., 2016. Biosens. Bioelectron. 79, 669–678.
Tiwari, J.N., Vij, V., Kemp, K.C., Kim, K.S., 2016. ACS Nano 10, 46–80.
Vabbina, P.K., Kaushik, A., Pokhrel, N., Bhansali, S., Pala, N., 2015. Biosens. Bioelectron. 63, 124–130.
Walling, C., 1975. Acc. Chem. Res. 8, 125–131.
Wan, Y., Su, Y., Zhu, X., Liu, G., Fan, C., 2013. Biosens. Bioelectron. 47, 1–11.
Wong, C.M., Wong, K.H., Chen, X.D., 2008. Appl. Microbiol Biotechnol. 78, 927–938.
Yang, W., Ratinac, K.R., Ringer, S.P., Thordarson, P., Gooding, J.J., Braet, F., 2010. Angew. Chem. Int. Ed. Engl. 49, 2114–2138.
Zheng, G.F., Patolsky, F., Cui, Y., Wang, W.U., Lieber, C.M., 2005. Nat. Biotechnol. 23, 1294–1301.